High-Current Vacuum Arc: The Relationship Between Anode Phenomena and the Average Opening Velocity of Vacuum Interrupters

Guowei Kong, Zhiyuan Liu, *Member, IEEE*, Dong Wang, and Mingzhe Rong, *Member, IEEE*

***Abstract*—In order to understand the influence of the average opening velocity on the high-current vacuum arc anode phenomena, high-speed photography was used to observe the anode phenomena of the vacuum arc discharge in vacuum interrupters. The contact diameters used in the vacuum interrupters were 12 and 25 mm, respectively. The contact materials included Cu, CuCr25, and CuCr50. The arc current frequency was 50 Hz, and the arcing time was controlled at about 9 ms. A permanent magnet mechanism with a contact spring was used to adjust the average opening velocity from 1.3 to 1.8 m/s. The experimental results showed that, with the arc current increasing, there was a threshold current I_{1st} (peak value) at which a high-current anode mode first appeared. Moreover, the first high-current anode mode was a footpoint at the velocity of 1.8 m/s, while, at the velocity of 1.3 m/s, it was most probably an anode spot and sometimes it was a footpoint. The result showed that, at the velocity of 1.8 m/s, the threshold current I_{1st} was lower than that at 1.3 m/s. Moreover, the threshold current I_{1st} followed the order of Cu $>$ CuCr25 $>$ CuCr50 at both the velocities of 1.3 m/s and 1.8 m/s. Meanwhile, at the higher average opening velocity of 1.8 m/s, the arc energy and arc voltage were higher than or close to those at 1.3 m/s.**

***Index Terms*—Anode phenomena, high current, opening velocity, vacuum arc, vacuum interrupters.**

I. Introduction

SINCE vacuum circuit breakers were first developed to interrupt short circuit current in the early 1960s [1], [2], the characteristics of high-current vacuum arcs have become an interesting research topic [3]–[8]. It is well known that the discharge mode transfers from a low-current mode to a high-current mode as the current exceeds a threshold level in a vacuum arc [9]–[14]. The anode plays an active role in the transition process of the discharge. Miller and Bellevue [10]–[13] pointed out that the vacuum arcs exhibit two low-current anode discharge modes and three high-current anode discharge modes. The transition from a low-current anode mode to a high-current anode mode depends on the contact material, the contact geometry (contact diameter, contact gap, etc.), and the current waveform [4], [15]. In the two low-current anode modes, the anode is basically passive, or the anode emits a flux of sputtered atoms. The three high-current anode discharge modes include a footpoint mode, an anode spot mode, and an intense arc mode [10]–[13]. In the three high-current anode discharge modes, there is a luminous region near the anode. The anode spot mode and the intense arc mode are accompanied with gross anode melting. In the footpoint mode, the anode melting is relatively small, occurring primarily at the footpoint site. If the power delivered to a footpoint exceeds the need of causing local melting, the footpoint temperature and erosion can increase rapidly. This could result in the formation of a small anode spot [10]–[13]. The temperature of a footpoint is near the melting point of the anode material, and the temperature of an anode spot is near the atmospheric boiling point of the anode material [10]–[12]. The formation of a high-current anode discharge mode is triggered by vapor emission from the anode, by magnetic constriction effects, or a combination of the two [11], [12]. Thus, a local anode surface is so hot that it evaporates a significant volume of metal vapor after current zero [15], [16]. When an appreciable transient recovery voltage appears across a contact gap, there is a critical value of metal vapor density to cause breakdown and failure [6], [17]. A liquid surface layer present at the melting anode area spot is also a possible cause of recovery failure. The old anode becomes the new cathode after current zero. If the transient recovery voltage applied is sufficiently strong, it can distort the liquid layer, pulling it into projections and thus creating points of high field concentration that are potential sites for high voltage breakdown [18]. The interaction between the liquid protrusion and metal vapor is suggested as a potential mechanism for a delayed breakdown [6], [17]. Moreover, the interaction also explains the post arc breakdown at high arc currents [19].

The parameters influencing the formation of an anode footpoint and/or an anode spot are well established [12], [15]. The critical current I_c [12] at which an anode spot forms increases with the anode diameter and decreases with the contact gap. When a contact material presents as a cathode material, the contact material that tends to produce greater densities of ions near the anode will result in higher values of I_c. However, when the contact material presents as an anode material, it will result in lower values of I_c [12]. An axial magnetic field, if applied to a vacuum arc, will shift the boundaries between the various modes to higher currents [13], [20].

Manuscript received September 30, 2010; revised December 15, 2010; accepted January 5, 2011. Date of publication March 10, 2011; date of current version June 10, 2011. This work was supported in part by the National Natural Science Foundation of China under Project 50537050 and in part by the Fundamental Research Funds For the Central Universities.

The authors are with the State Key Laboratory of Electrical Insulation and Power Equipment, Department of Electrical Engineering, Xi'an Jiaotong University, Xi'an 710049, China (e-mail: kgw.fb@stu.xjtu.edu.cn; liuzy@mail.xjtu.edu.cn).

Color versions of one or more of the figures in this paper are available online at http://ieeexplore.ieee.org.

Digital Object Identifier 10.1109/TPS.2011.2107529

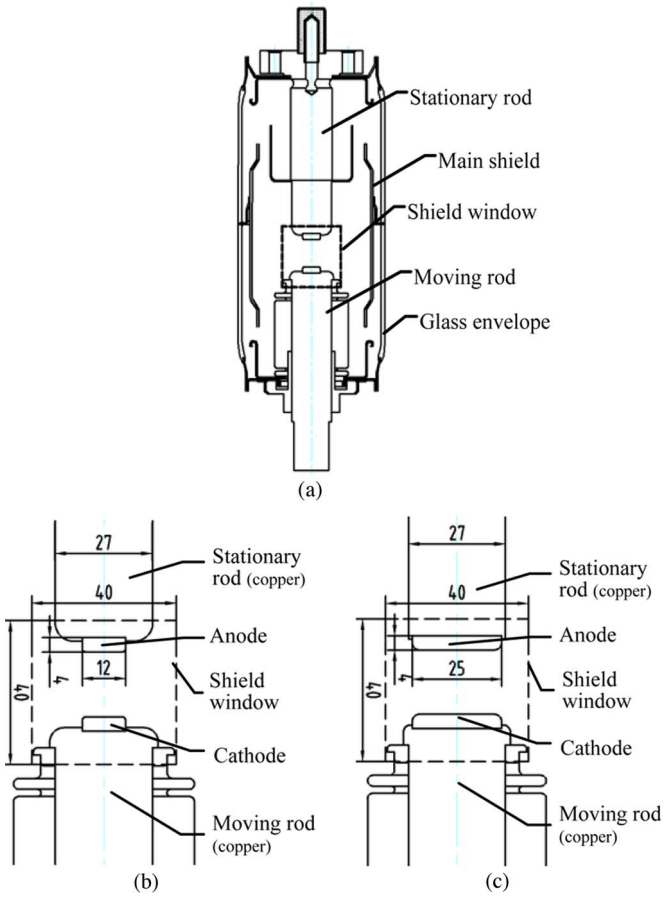

Fig. 1. Vacuum interrupter and electrodes in experiment. (a) Vacuum interrupter. (b) Contact diameter of 12 mm. (c) Contact diameter of 25 mm.

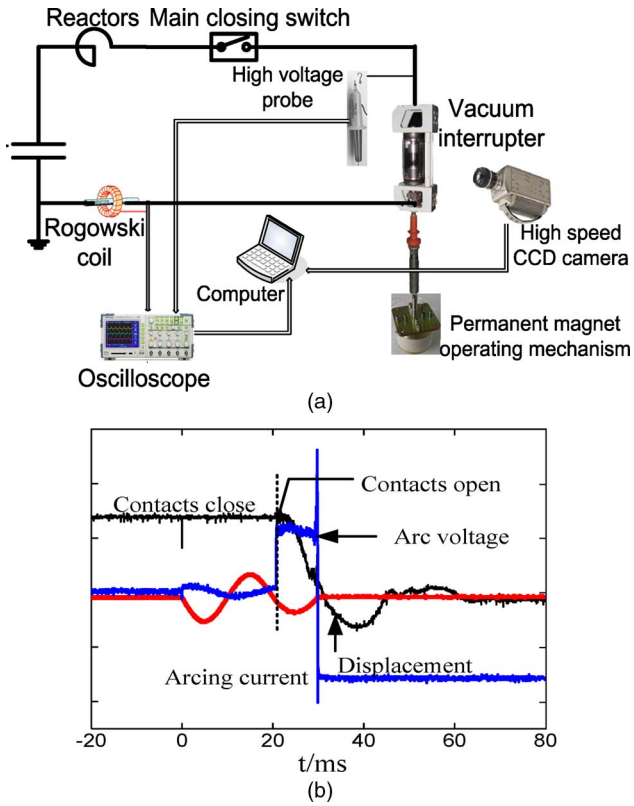

Fig. 2. Experimental setup for an anode phenomenon observation. (a) Experimental circuit. (b) Waveform of arc current, arc voltage, and displacement curve of moving contact.

When a vacuum circuit breaker receives a trip signal to interrupt a current, the contacts will be separated by an operating mechanism. Then, a drawing arc is initiated between a pair of electrodes. An opening velocity characteristic was reported as a contributing factor for improving the high-current interruption performance of a vacuum circuit breaker [21], [22]. However, how the opening velocity characteristic influences high-current vacuum arc behaviors, particularly the high-current vacuum arc anode phenomena in vacuum interrupters, is unknown.

The purpose of this paper is to understand the influence of opening velocities on the high-current vacuum arc anode phenomena. In this paper, we focus on the influence of average opening velocities on a threshold current I_{1st} (peak value) with which a high-current anode phenomenon first appears. The experimental results may provide an elaboration of a dynamic model of high-current vacuum arc anode discharge phenomena.

II. Experimental Setup

Experiments were conducted to understand the influence of the average opening velocity on the high-current vacuum arc anode phenomena. In the experiments, the vacuum interrupters shown in Fig. 1(a) were used for the anode phenomenon observation. The vacuum interrupters were sealed before testing. For the purpose of arc observation, the envelope of the vacuum interrupter was made of glass, and there was an observation window (40 mm $\times$ 40 mm) on the stainless steel shield of the vacuum interrupter. Therefore, anode phenomena can be observed by high-speed photography. The high-speed charge-coupled-device video camera Phantom V10 was used to record the vacuum arc mode evolution in the experiments. The recording velocity was set to be 4000 frames/s. The camera aperture was fixed at four, and the exposure time for a fresh vacuum interrupter was set as 2 μs. After successive current interruptions, there were continuous metal vapor depositions on the glass envelope of the vacuum interrupter. Therefore, the exposure time was adjusted according to the metal vapor depositions on the glass envelope. Fig. 1(b) shows the butt-type electrodes in the vacuum interrupters. The diameters of the electrodes were 12 and 25 mm, respectively. The thickness of the electrode was 4 mm. Three kinds of contact materials were used: oxygen-free high-conductivity copper, CuCr25 (25% Cr), and CuCr50 (50% Cr). The contact gap was 18 mm. In the experiments, the upper electrode was the anode.

The experiments were conducted using the apparatus shown schematically in Fig. 2(a). A drawn arc was initiated between a pair of butt electrodes in the vacuum interrupter shown in Fig. 1(a). The opening velocity of the movable electrode in the vacuum interrupter was adjusted by a contact spring of a permanent magnet operating mechanism. The displacement signal of the movable electrode in an opening operation was measured by a KTC-100-type linear displacement transducer.

Tests were conducted by charging capacitor banks to an appropriate voltage and initiating a power frequency current

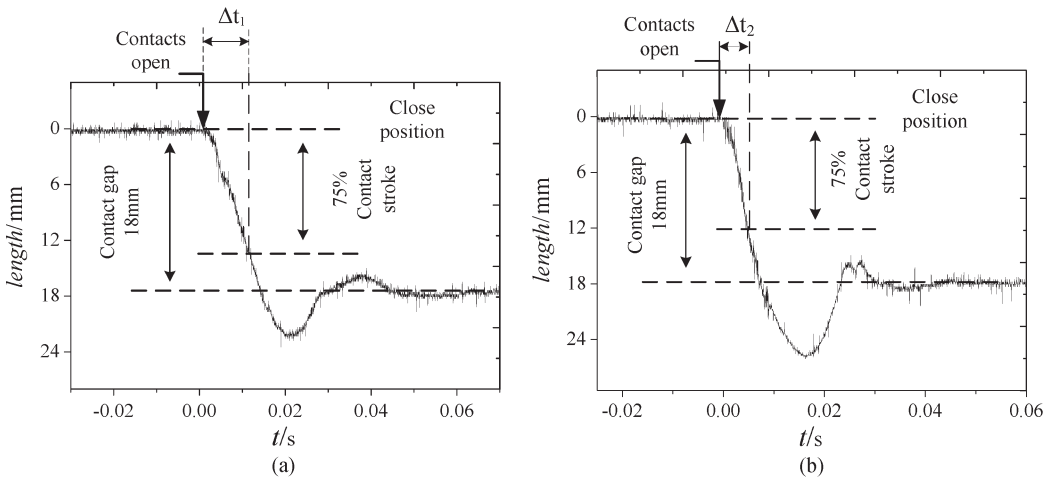

Fig. 3. Definition of an average opening velocity. Time of 75% range of the contact gap: $\Delta t_1 > \Delta t_2$. (a) Opening displacement curve at 1.3 m/s. (b) Opening displacement curve at 1.8 m/s.

TABLE I
ARC CURRENT IN THE EXPERIMENTS

Contact material	Contact Diameter (mm)	Average opening velocity (m/s)	Peak value of arc current (kA)								
			I	II	III	IV	V	VI	VII	VIII	IX
Cu	12	1.3	0.54	1.36		2.84	3.24	4.15#	4.44	5.28	5.68
		1.8	0.62		2.08		3.42#	4.10			
	25	1.3		2.48		3.88	4.64	5.36	5.92#	6.88	7.76
		1.8	1.06	2.64		4.08	4.72#	5.46			
CuCr25	12	1.3		1.22	1.82	2.46	2.91#	4.08	4.96		
		1.8		1.28	1.76	2.29#	3.20				
CuCr50	12	1.3	0.60	1.24	1.84	2.64#	3.18				
		1.8	0.51	1.21	1.76	2.48#	2.86	3.42			
	25	1.3	0.76	2.38	3.04	3.68#	4.23	5.06			
		1.8	0.92	2.31	2.88#	3.25	3.84				

Threshold level of arc current, at which discharge mode transfers from a low-current mode to a high-current mode.

(50 Hz) by passing through reactors ($L-C$ discharging circuit). The discharging current was controlled by the charging voltage. As shown in Fig. 2(b), while the electrodes were kept closed in the first and the second half-wave of the 50-Hz power frequency current, the movable electrode was electronically controlled to be separated within the first millisecond of the third half-wave of the initiated current. Thus, the arcing time in each experiment was about 9 ms when the arc extinguished at the first arc current zero point. The arc voltage was measured by means of a Tektronix high-voltage probe 6015A (1000:1), and the arc current was measured by a Rogowski coil and/or a shunt of 80 $\mu\Omega$. Three measured signals—the displacement of a movable electrode, the arc current, and the arc voltage—were sent to an oscilloscope for recording, as shown in Fig. 2(b).

Fig. 3 shows an opening displacement curve of the movable electrode. The average opening velocity was defined as an average velocity within the 75% range of the contact gap (18 mm) from the point of contact departure. For the permanent magnet operating mechanism that we used, the average opening velocity can be adjusted from 1.3 to 1.8 m/s by adjusting its contact spring stroke from 1 to 6.5 mm. Thus, the two average opening velocities (1.3 and 1.8 m/s) were adopted to compare their influence on the high-current vacuum arc anode phenomena.

TABLE II
CHARACTERISTICS OF FOOTPOINT AND ANODE SPOT

Mode	Arc voltage noise	Luminous area on anode	Interelectrode gap plasma	Plasma concentration on electrodes
Footpoint	high	small size and moderate bright	diffuse	only anode
Anode spot	moderate high	large size and bright	columnar or jet arc	anode and cathode

Table I shows the arc current applied in the experiments. The experiments started from a low current level (the peak current was several hundreds of amperes) in a vacuum interrupter, at which the anode was passive. Therefore, the arc discharge was a low-current anode mode. Thereafter, the arc current was increased in the vacuum interrupter following the sequence of groups I, II, III, . . . , IX. Then, the vacuum interrupters with different contact materials (Cu, CuCr25, and CuCr50)

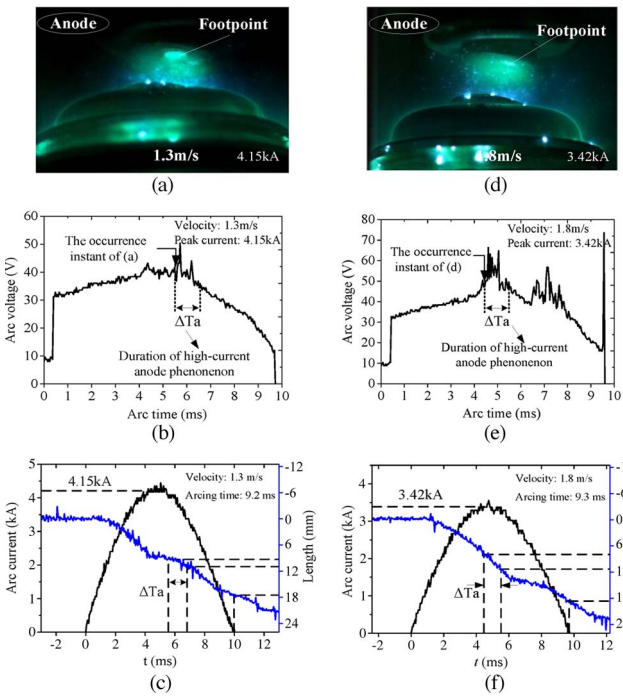

Fig. 4. First high-current anode phenomena of Cu, with a contact diameter of 12 mm. (Left column) 1.3 m/s. (Right column) 1.8 m/s. (a) First high-current anode mode at 1.3 m/s, with a peak arc current of 4.15 kA. (b) Arc voltage waveform at 1.3 m/s, with a peak current of 4.15 kA. (c) Arc current waveform and contact stroke at 1.3 m/s, with a peak current of 4.15 kA. (d) First high-current anode mode at 1.8 m/s, with a peak arc current of 3.42 kA. (e) Arc voltage waveform at 1.8 m/s, with a peak current of 3.42 kA. (f) Arc current waveform and contact stroke at 1.8 m/s, with a peak current of 3.42 kA.

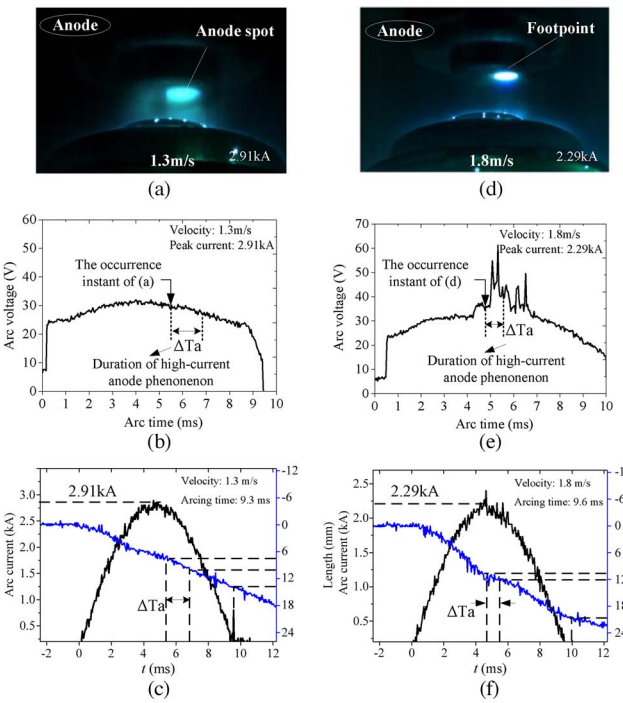

Fig. 5. First high-current anode phenomena of CuCr25, with a contact diameter of 12 mm. (Left column) 1.3 m/s. (Right column) 1.8 m/s. (a) First high-current anode mode at 1.3 m/s, with a peak arc current of 2.91 kA. (b) Arc voltage waveform at 1.3 m/s, with a peak current of 2.91 kA. (c) Arc current waveform and contact stroke at 1.3 m/s, with a peak current of 2.91 kA. (d) First high-current anode mode at 1.8 m/s, with a peak arc current of 2.29 kA. (e) Arc voltage waveform at 1.8 m/s, with a peak current of 2.29 kA. (f) Arc current waveform and contact stroke at 1.8 m/s, with a peak current of 2.29 kA.

and different contact diameters (12 and 25 mm) were tested in the set sequences of the arc current until the first high-current anode phenomenon occurred. The arc current variation at each arc current level was controlled to be less than 10%, so the experimental results were comparable in different contact materials (Cu, CuCr25, and CuCr50) and in different average opening velocities (1.8 and 1.3 m/s).

III. Experimental Results

A. High-Current Vacuum Arc Anode Phenomena

As the arc current increases, the first high-current vacuum arc anode phenomenon observed in our experiment is a footpoint or an anode spot. In this paper, we followed the following definition of Miller and Bellevue [13] to determine the footpoint or anode spot.

In the footpoint mode, the interelectrode gap is mostly filled with a fairly bright diffuse glow (appearing much the same as the diffuse arc mode at higher currents). However, in contrast to the diffuse arc mode, where the anode is nonluminous, in the footpoint mode, small bright spots appear on the anode. These spots are denoted as footpoints. Footpoints are characterized as being small luminous spots, usually associated with local anode melting and with the appearance of anode material in the discharge.

The anode spot mode is a high-current mode with considerable anode activity. In the anode spot mode, a more or less well-defined arc column appears in the interelectrode gap, while many (perhaps individually indistinguishable) cathode spots cover the cathode. One large or (less often) several small very bright spots are present on the anode.

Based on the definition of a footpoint and an anode spot by Miller and Bellevue [13], we determined a footpoint and an anode spot in our experiments by using the characteristics described in Table II. A footpoint met the following criteria at the same time: 1) There is a small bright region on the anode; 2) the arc voltage noise is high; and 3) there is a diffuse arc in the interelectrode gap. In the meantime, an anode spot met the following criteria at the same time: 1) There is a large bright region; 2) the arc voltage noise is moderately high; and 3) there is a columnar arc or jet arc in the interelectrode gap.

Figs. 4–8 compare the first high-current anode phenomena at the average opening velocities of 1.3 and 1.8 m/s in the experiment. The first high-current anode phenomena included the arc appearance, arc voltage waveform, and contact stroke curve. Figs. 4–6 show the cases of the contact diameter of 12 mm, and the contact materials are Cu, CuCr25, and CuCr50, respectively. Figs. 7 and 8 show the cases of the contact diameter of 25 mm, and the contact materials are Cu and CuCr50, respectively. The duration of the high-current anode phenomenon ΔT_a was indicated in the arc voltage waveform and in the contact stroke curve. During ΔT_a, the high-current anode mode could keep or transfer to a footpoint or an anode spot, depending on different arc currents and contact strokes. The occurrence instant of the high-current anode phenomenon was also given in the arc voltage waveform, before which there was no

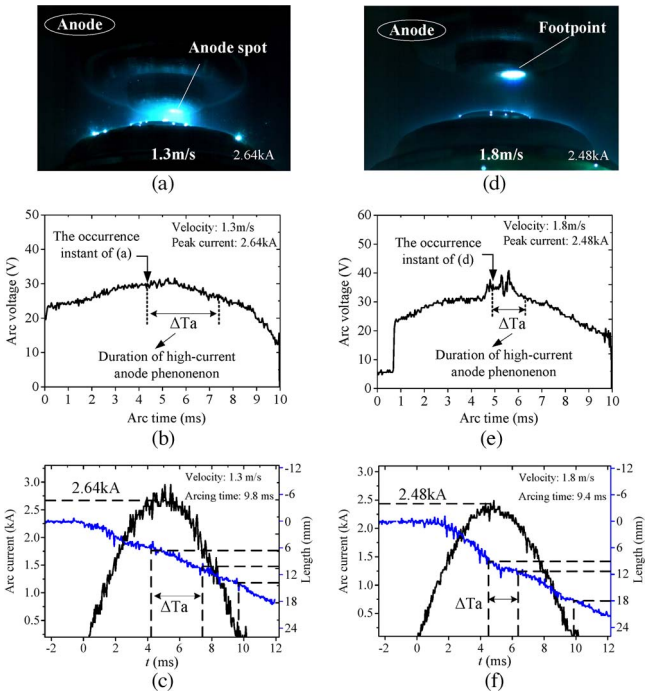

Fig. 6. First high-current anode phenomena of CuCr50, with a contact diameter of 12 mm. (Left column) 1.3 m/s. (Right column) 1.8 m/s. (a) First high-current anode mode at 1.3 m/s, with a peak arc current of 2.64 kA. (b) Arc voltage waveform at 1.3 m/s, with a peak current of 2.64 kA. (c) Arc current waveform and contact stroke at 1.3 m/s, with a peak current of 2.64 kA. (d) First high-current anode mode at 1.8 m/s, with a peak arc current of 2.48 kA. (e) Arc voltage waveform at 1.8 m/s, with a peak current of 2.48 kA. (f) Arc current waveform and contact stroke at 1.8 m/s, with a peak current of 2.48 kA.

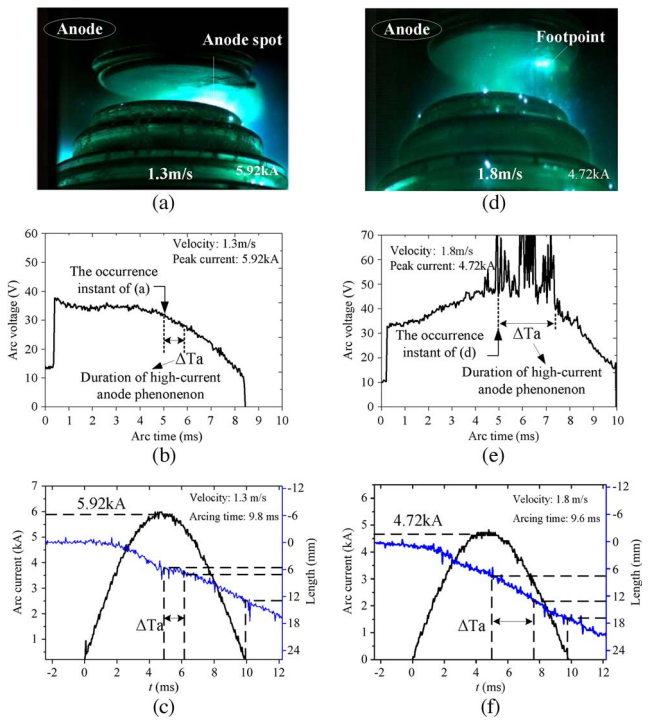

Fig. 7. First high-current anode phenomena of Cu with a contact diameter of 25 mm. (Left column) 1.3 m/s. (Right column) 1.8 m/s. (a) First high-current anode mode at 1.3 m/s, with a peak arc current of 5.92 kA. (b) Arc voltage waveform at 1.3 m/s, with a peak current of 5.92 kA. (c) Arc current waveform and contact stroke at 1.3 m/s, with a peak current of 5.92 kA. (d) First high-current anode mode at 1.8 m/s, with a peak arc current of 4.72 kA. (e) Arc voltage waveform at 1.8 m/s, with a peak current of 4.72 kA. (f) Arc current waveform and contact stroke at 1.8 m/s, with a peak current of 4.72 kA.

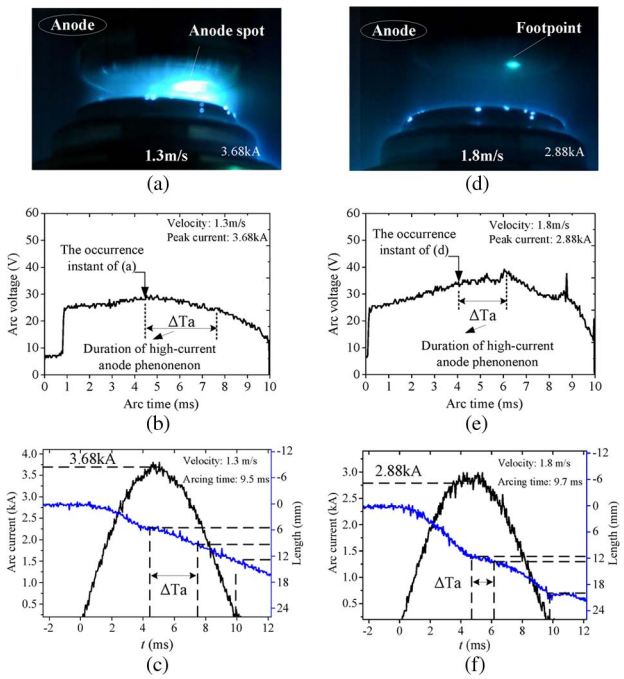

Fig. 8. First high-current anode phenomena of CuCr50 with a contact diameter of 25 mm. (Left column) 1.3 m/s. (Right column) 1.8 m/s. (a) First high-current anode mode at 1.3 m/s, with a peak arc current of 3.68 kA. (b) Arc voltage waveform at 1.3 m/s, with a peak current of 3.68 kA. (c) Arc current waveform and contact stroke at 1.3 m/s, with a peak current of 3.68 kA. (d) First high-current anode mode at 1.8 m/s, with a peak arc current of 2.88 kA. (e) Arc voltage waveform at 1.8 m/s, with a peak current of 2.88 kA. (f) Arc current waveform and contact stroke at 1.8 m/s, with a peak current of 2.88 kA.

high-current anode phenomenon found. Arcing photographs at the occurrence instant were displayed in Figs. 4–8. Moreover, the opening displacement at the time of current zero was indicated in the contact stroke curve. By the definition of a footpoint and an anode spot mentioned earlier, the first high-current anode phenomenon that took place was most probably an anode spot (sometimes a footpoint) mode at 1.3 m/s, and it was a footpoint mode at 1.8 m/s.

B. *Threshold Current* I_{1st}

We defined the peak arc current at which a high-current anode phenomenon (footpoint or anode spot) first appeared as a *threshold current* I_{1st}. Fig. 9 shows the *threshold current* I_{1st} at the average opening velocities of 1.3 and 1.8 m/s with contact materials Cu, CuCr25, and CuCr50 and contact diameters of 12 and 25 mm. In Fig. 9, the triangle denotes a footpoint, and the circle denotes an anode spot. Fig. 9 shows that the *threshold current* I_{1st} was higher at the average opening velocity of 1.3 m/s than that at 1.8 m/s no matter what contact material or contact diameter is involved in the experiment. Moreover, it also shows that I_{1st} followed the order of Cu $>$ CuCr25 $>$ CuCr50 [see Fig. 9(a)] and Cu $>$ CuCr50 [see Fig. 9(b)] at both velocities. Meanwhile, Fig. 9 shows that, as the arc current increases, the high-current anode mode that first appeared was a footpoint at the opening velocity of 1.8 m/s, regardless of the type of the contact material, being Cu, CuCr25, and CuCr50, and the size of the contact diameter, being 12 and 25 mm. At the average opening velocity of 1.3 m/s, the high-current anode mode that first appeared was most probably an anode spot, and

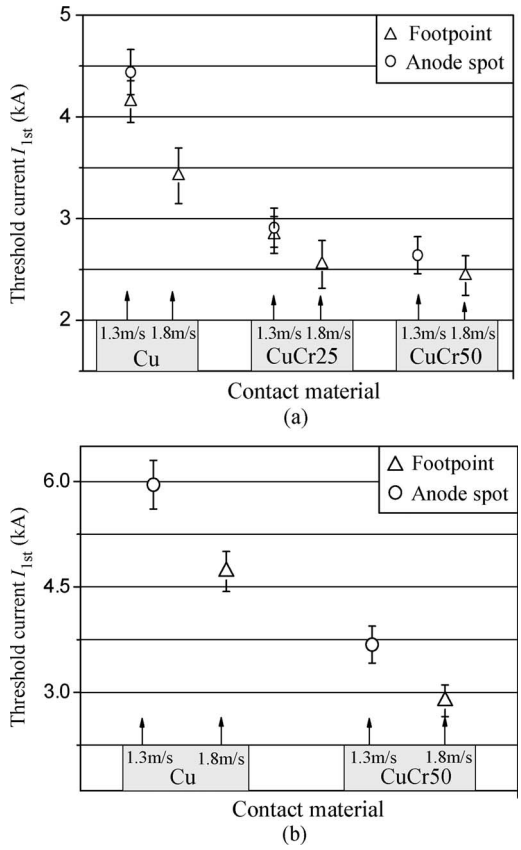

Fig. 9. Diagram of threshold currents. As the arc current increases, there appears the first high-current anode mode at the threshold current I_{1st}. (a) Contact diameter of 12 mm. (b) Contact diameter of 25 mm.

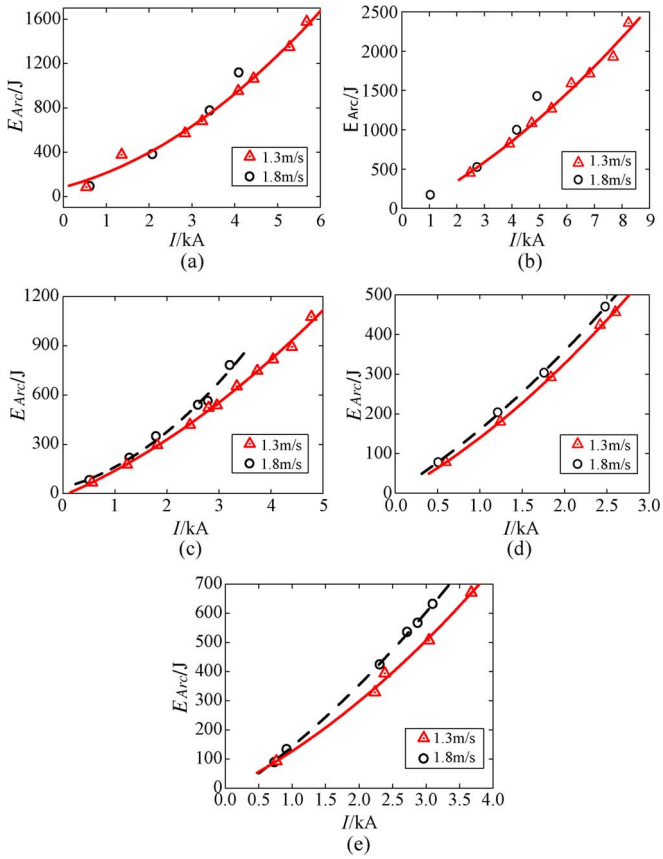

Fig. 10. Arc energy at the average opening velocities of 1.3 and 1.8 m/s. Current label—peak arc current. (a) Cu, Φ12 mm. (b) Cu, Φ25 mm. (c) CuCr25, Φ12 mm. (d) CuCr50, Φ12 mm. (e) CuCr50, Φ25 mm.

sometimes, it was a footpoint. However, the threshold current I_{1st} of the footpoint was close to that of the anode spot at the average opening velocity of 1.3 m/s.

C. Arc Energy

The arc energy is calculated from the arc current and arc voltage by the integration of the arcing time. In the experiment, we calculated the arc energy during the arcing time that was 9 ms. Fig. 10 illustrates the arc energy at the average opening velocities of 1.3 and 1.8 m/s. Fig. 10(a) and (b) presents two cases with Cu being the contact material. Fig. 10(a) shows the case with a contact diameter of 12 mm, and Fig. 10(b) shows the case with a contact diameter of 25 mm. Fig. 10(a) and (b) shows that, at the velocity of 1.3 m/s, the arc energy was close to that at 1.8 m/s. Fig. 10(c) illustrates the case of the contact material being CuCr25 with a contact diameter of 12 mm. Fig. 10(d) and (e) shows the cases with the contact material being CuCr50 and with the contact diameters being 12 and 25 mm, respectively. Fig. 10(c)–(e) shows that, at the average opening velocity of 1.8 m/s, the arc energy was higher than that at 1.3 m/s, particularly in the high-current range. Therefore, the result indicated that, at the velocity of 1.8 m/s, the arc voltage was higher than or close to that at 1.3 m/s at the same arc current.

By a regression analysis, it was found that the relationship between the arc energy and the peak arc current followed

$$E_{\text{arc}} = a + b^{c} \tag{1}$$

TABLE III
POWER FACTOR c IN (1)

Contact diameter	12 mm			25 mm	
Contact material	Cu	CuCr25	CuCr50	Cu	CuCr50
1.3 m/s	1.61	1.36	1.36	1.41	1.41
1.8 m/s	1.88	1.65	1.29	2.15	1.30

where

E_{arc} arc energy (in joules);
I peak value of arc current (in kiloamperes);
a, b, and c constant.

Table III shows the power factor c in (1). It was found that, at the average opening velocity of 1.8 m/s, the power factor c followed the order Cu > CuCr25 > CuCr50, with the contact diameters being 12 and 25 mm, respectively. However, at the average opening velocity of 1.3 m/s, the power factor c tended to be close to each other.

IV. DISCUSSION

A. Anode Modes at the Threshold Current I_{1st}

The experimental results showed that the high-current anode mode that first appeared was a footpoint at the opening velocity of 1.8 m/s, regardless of the type of the contact material,

being Cu, CuCr25, and CuCr50, and the size of the contact diameter, being 12 and 25 mm. In the footpoint mode, there was a small-size luminous spot on the anode. Moreover, there was a diffuse arc between the contact gaps in the footpoint mode. However, at the velocity of 1.3 m/s, the high-current anode mode that first appeared was most probably an anode spot with the arc current increasing. There was a large bright spot on the anode. Moreover, there was a columnar or jet arc with a distinguishable boundary between the contacts in the anode spot mode. These phenomena could be explained by the following: With the high average opening velocity of 1.8 m/s, a footpoint formed due to the "*instability of the anode sheath*" [6] (also known as "*ion starvation*" [9]). Because a high velocity corresponded to a high contact gap at which the density of the plasma adjacent to the anode was too low, the ion starvation current incident on the anode was smaller for the higher contact gap [9]. However, at the low average opening velocity of 1.3 m/s, the anode transition was related to the "*gas-dynamic*" effect [15]. In such a case, the contact gap was comparably low. The stability of the cathode spot or group spot (appearing to cover the anode and the cathode) determined the arc characteristics, including the electrode erosion, density and temperature of interelectrode gap plasma, etc. The state of the arc characteristics consequently influenced the anode transition phenomena. Therefore, the experimental results supported the theory well.

Sometimes, the high-current anode mode that first appeared was a footpoint at the average opening velocity of 1.3 m/s. This is probably related to the contact material and contact diameter. Compared with CuCr50, Cu, and CuCr25 were more likely to form a footpoint. Moreover, the possibility of a footpoint formation for Φ12 mm is greater than that for Φ25 mm.

B. Anode Voltage

The experimental results of the arc voltage noise agreed with that of Miller. Miller and Bellevue [13] mentioned that the footpoint was accompanied with an appreciable noise component of the arc voltage. The experimental results followed the description of Miller well. Meanwhile, he also mentioned that the presence or absence of an anode jet might have a significant effect upon the arc voltage noise of the anode spot, but the evidence of the arc voltage noise that he got was contradictory [13]. In order to explain it, Miller and Bellevue [13] referred to the comments of Boxman and Harris that the appearance of an anode jet had little effect upon the arc voltage (mean value or noise component) unless the anode jet either struck the cathode or met a cathode jet.

Our experimental results supported the aforementioned explanation. Fig. 11 shows the high-current arc phenomena with the intersection of the anode jet and the cathode jet. Compared with Figs. 4(a)–8(a), the anode jet and the cathode jet come to intersect in Fig. 11(a) and (c). The arc voltage waveforms in the cases of Figs. 4(a)–8(a) are shown in Figs. 4(b)–8(b), respectively. Figs. 4(b)–8(b) show that there was lower significant arc voltage noise when there was no meeting of the anode jet and the cathode jet. The arc voltage waveforms in the cases of Fig. 11(a) and (c) are shown in Fig. 11(b) and (d), respectively.

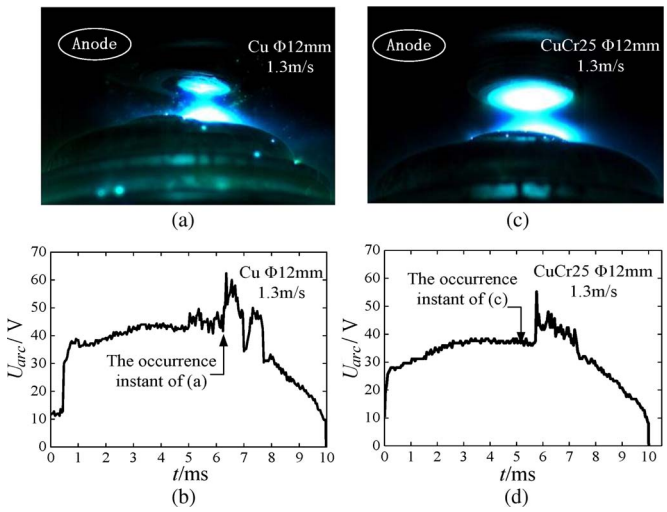

Fig. 11. High-current arc phenomena with the intersection of the anode jet and the cathode jet. (a) One appearance of arc phenomenon, with Cu, Φ12 mm, and a peak current of 5.68 kA. (b) Arc voltage waveform, with Cu, Φ12 mm, and a peak current of 5.68 kA. (c) One appearance of arc phenomenon, with CuCr25, Φ12 mm, and a peak current of 4.96 kA. (d) Arc voltage waveform, with CuCr25, Φ12 mm, and a peak current of 4.96 kA.

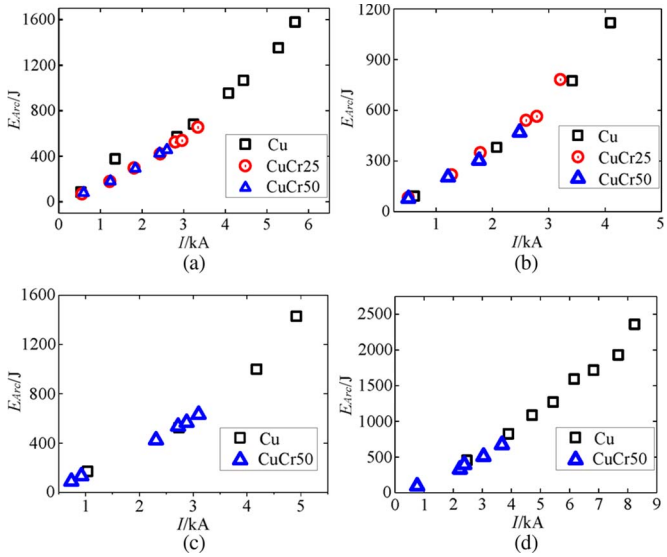

Fig. 12. Comparison of arc energy among contact materials Cu, CuCr25, and CuCr50. Current label—peak arc current. (a) 1.3 m/s, Φ12 mm. (b) 1.8 m/s, Φ12 mm. (c) 1.3 m/s, Φ25 mm. (d) 1.8 m/s, Φ25 mm.

Fig. 11(b) and (d) shows that there was significant arc voltage noise when the anode jet met a cathode jet. Therefore, our experimental results validated the correctness of the explanation.

C. Contact Material and Anode Energy

Fig. 12 compares the arc energy among the contact materials, being Cu, CuCr25, and CuCr50. Fig. 12 shows that the arc energy curves were close to each other when the contact materials were Cu, CuCr25, and CuCr50, respectively, at the same average opening velocity of 1.8 or 1.3 m/s. However, the maximum arc energy of the CuCr25 and CuCr50 contact materials was lower than that of Cu. This was in accordance

with the CuCr25 and CuCr50 contact materials having a lower threshold current (see Fig. 9).

D. Contact Material and High Current Interruption

Fig. 9 shows that the threshold current was in the order of $\mathrm{Cu} > \mathrm{CuCr25} > \mathrm{CuCr50}$ with the same average opening velocity. This means that the Cu contact material had the highest threshold current $I_{1\mathrm{st}}$. This result is contradictory to the knowledge that the CuCr family has a higher interrupting capacity than Cu. A possible explanation is that the addition of Cr dramatically reduces the thermal conductivity of the CuCr composite. Typically, from 25 wt% Cr to 50 wt% Cr, the thermal conductivity is reduced by about 40%–50%, depending on the density and mutual solid solution between Cu and Cr [23].

Another possible explanation is the presence of metal droplets in the contact gap. In the experiment, there was a more significant amount of visible metal droplets in the Cu contact gaps than in the CuCr family contact gaps. Therefore, even though Cu has a higher threshold current at which a high-current anode mode first appears, it has a lower interrupting capacity than the CuCr family because the metal droplets will live after current zero, which evidently has a significant impact on the dielectric recovery strength of vacuum interrupters.

Sugita *et al.* [24] also reported the same finding. They observed many bright points in the vacuum arcs of Cu. They thought the insulation ability became worse when a certain level of particles existed between the electrodes. As a result, they considered that the contact materials are unfit for high-voltage use. They also pointed that the bright points or particles were not observed in the vacuum arc of the CuCr family. Therefore, metal particles could be one of the key influencing factors to the high current interrupting capacity of vacuum interrupters.

E. Average Opening Velocity and High Current Interruption

Fig. 9 shows that, at the average opening velocity of 1.8 m/s, the threshold $I_{1\mathrm{st}}$ current was lower than that at 1.3 m/s. The result that a higher opening velocity has a lower threshold current seemed to contradict with the knowledge that a higher opening velocity improves the interruption capacity of a vacuum circuit breaker. The explanation could be that the first high-current anode mode that appeared was a footpoint at 1.8 m/s and it was an anode spot at 1.3 m/s. Therefore, the anode spot evaporated much more metal vapors than the footpoint, and the more metal vapors contributed to the interruption failures. Therefore, a higher average opening velocity corresponded to a higher interrupting capacity, so the metal vapor density should be a key influencing factor to the interrupting capacity of vacuum interrupters.

V. Conclusion

We have experimentally observed the high-current anode phenomena at the average opening velocities of 1.8 and 1.3 m/s by using vacuum interrupters that were sealed off before testing. The contact diameters were 12 and 25 mm, respectively. The contact materials included Cu, CuCr25, and CuCr50. The arc current frequency was 50 Hz. The experimental results showed that, as the arc current increases, the high-current anode mode that first appeared was a footpoint at the average opening velocity of 1.8 m/s. However, at the velocity of 1.3 m/s, the high-current anode mode that first appeared was most probably an anode spot, and sometimes, it was a footpoint. This result provided a support to the arc transition theory of Schade that, at the high velocity of 1.8 m/s, a footpoint was formed by the effects of the "*instability of the anode sheath*," and at the low velocity of 1.3 m/s, an anode spot was formed by the effects of "*gas dynamic*."

By the definition of a threshold current $I_{1\mathrm{st}}$ (peak current value) with which the high-current anode mode first appeared, the results showed that the threshold current $I_{1\mathrm{st}}$ followed the relationship of $I_{1\mathrm{st}}\ (1.3\ \mathrm{m/s}) > I_{1\mathrm{st}}\ (1.8\ \mathrm{m/s})$. Moreover, the threshold current $I_{1\mathrm{st}}$ followed the order of $\mathrm{Cu} > \mathrm{CuCr25} > \mathrm{CuCr50}$ at both velocities of 1.3 and 1.8 m/s. This result seems contradictory to the knowledge that the CuCr family has a higher interrupting capacity than Cu and the knowledge that a higher opening velocity improves the interruption capacity of a vacuum circuit breaker. It was considered that metal droplet quantities and metal vapor density played important roles in the high current interrupting process of vacuum interrupters. The results also indicated that, at the average opening velocity of 1.8 m/s, the arc voltage and energy were higher than or close to those at 1.3 m/s.

References

[1] T. H. Lee, A. N. Greenwood, D. W. Crouch, and C. H. Titus, "Development of power vacuum interrupters," *AIEE Trans. Power App. Syst.*, vol. 81, no. 3, pp. 629–636, Apr. 1962.

[2] R. Boxman, S. Goldsmith, and A. Greenwood, "Twenty-five years of progress in vacuum arc research and utilization," *IEEE Trans. Plasma Sci.*, vol. 25, no. 6, pp. 1174–1186, Dec. 1997.

[3] J. M. Lafferty, Ed., *Vacuum Arcs Theory and Application*. New York: Wiley, 1980.

[4] R. L. Boxman, P. J. Martin, and D. M. Sanders, Eds., *Handbook of Vacuum Arc Science and Technology Fundamentals and Applications*. Park Ridge, NJ: Noyes, 1995.

[5] P. G. Slade, *The Vacuum Interrupter Theory, Design, and Application*. Boca Raton, FL: CRC Press, 2008.

[6] E. Schade, "Physics of high-current interruption of vacuum circuit breakers," *IEEE Trans. Plasma Sci.*, vol. 33, no. 5, pp. 1564–1575, Oct. 2005.

[7] M. Binnendijk, W. Merck, R. Smeets, K. Watanabe, and E. Kaneko, "High-current interruption in vacuum circuit breakers," *IEEE Trans. Dielectr. Elect. Insul.*, vol. 4, no. 6, pp. 836–840, Dec. 1997.

[8] E. Schade and D. Dullni, "Investigation of high-current interruption of vacuum circuit breakers," *IEEE Trans. Dielectr. Elect. Insul.*, vol. 28, no. 4, pp. 607–620, Aug. 1993.

[9] C. W. Kimblin, "Anode voltage drop and anode spot formation in dc vacuum arc," *J. Appl. Phys.*, vol. 40, no. 4, pp. 1744–1750, Mar. 1969.

[10] H. C. Miller, "Vacuum arc anode phenomena," *IEEE Trans. Plasma Sci.*, vol. PS-11, no. 2, pp. 76–89, Jun. 1983.

[11] H. C. Miller, "Discharge modes at the anode of a vacuum arc," *IEEE Trans. Plasma Sci.*, vol. PS-11, no. 3, pp. 122–127, Sep. 1983.

[12] H. C. Miller, "A review of anode phenomena in vacuum arcs," *IEEE Trans. Plasma Sci.*, vol. PS-13, no. 5, pp. 242–252, Oct. 1985.

[13] H. C. Miller and W. A. Bellevue, "Anode modes in vacuum arcs," *IEEE Trans. Dielectr. Elect. Insul.*, vol. 4, no. 4, pp. 382–388, Aug. 1997.

[14] E. F. Prozorov, D. K. Ulyanov, K. N. Ulyanov, and V. A. Fedorov, "Experimental study of dynamics of plasma expansion in a vacuum-arc discharge and anode temperature calculations," *IEEE Trans. Plasma Sci.*, vol. 37, no. 8, pp. 1398–1402, Aug. 2009.

[15] I. I. Beilis, "State of the theory of vacuum arcs," *IEEE Trans. Plasma Sci.*, vol. 29, no. 5, pp. 657–670, Oct. 2001.

[16] E. Schade and D. Shmelev, "Numerical simulation of high-current vacuum arcs in external magnetic fields taking into account essential anode evaporation," in *Proc. 21st Int. Symp. Discharges Elect. Insul. Vac.*, Yalta, Ukraine, 2004, pp. 411–414.
[17] E. Schade and D. Dullni, "Recovery of breakdown strength of a vacuum interrupter after extinction of high currents," *IEEE Trans. Dielectr. Elect. Insul.*, vol. 9, no. 2, pp. 207–215, Apr. 2002.
[18] H. C. Miller, "Vacuum arc anode phenomena," *IEEE Trans. Plasma Sci.*, vol. PS-5, no. 3, pp. 181–196, Sep. 1977.
[19] S. W. Rowe, "The intrinsic limits of vacuum interruption," in *Proc. 23rd Int. Symp. Discharges Elect. Insul. Vac.*, Bucharest, Romania, 2008, pp. 192–197.
[20] Y. Matsui, A. Sano, H. Komatsu, H. Satou, and H. Saito, "Vacuum arc phenomena under various axial magnetic field and anode melting," in *Proc. 24th Int. Symp. Discharges Elect. Insul. Vac.*, Braunschweig, Germany, 2010, pp. 324–327.
[21] S. Yuan, Y. Wang, and J. Wang, "Optimal moving curve of electrode to interrupt a short current for vacuum circuit breaker," in *Proc. 2nd Int. Symp. ECAAA*, Xi'an, China, 1993, pp. 248–251.
[22] J. Kusserow and R. Renz, "Method for opening the contact gap of a vacuum interrupter," U.S. Patent 7 334 319, Feb. 26, 2008.
[23] W. Li, R. L. Thomas, and R. K. Smith, "Effects of Cr content on the interruption ability of CuCr contact materials," *IEEE Trans. Plasma Sci.*, vol. 29, no. 5, pp. 744–748, Oct. 2001.
[24] M. Sugita, S. Okabe, G. Ueta, W. Wang, X. Wang, and S. Yanabu, "Interruption phenomena for various contact materials in vacuum," *IEEE Trans. Plasma Sci.*, vol. 37, no. 8, pp. 1469–1476, Aug. 2009.

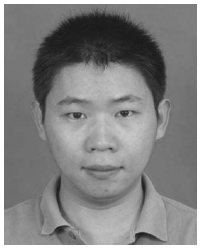

Guowei Kong was born in Henan Province, China, in 1985. He received the B.S. degree in electrical engineering from the Shenyang University of Technology, Liaoning, China, in 2008. Since then, he has studied in Xi'an Jiaotong University, Xi'an, China, where he is currently working toward the Ph.D. degree in the State Key Laboratory of Electrical Insulation and Power Equipment, Department of Electrical Engineering.

His research interests focus on vacuum arcs and vacuum circuit breakers.

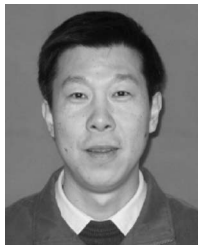

Zhiyuan Liu (M'01) was born in Shenyang, China, in 1971. He received the B.S. and M.S. degrees in electrical engineering from the Shenyang University of Technology, Liaoning, China, in 1994 and 1997, respectively, and the Ph.D. degree in electrical engineering from Xi'an Jiaotong University, Xi'an, China, in 2001.

From 2001 to 2002, he was with the General Electric Company Research and Development Center (Shanghai), Shanghai, China. Since 2003, he has been with the State Key Laboratory of Electrical Insulation and Power Equipment, Department of Electrical Engineering, Xi'an Jiaotong University, where he is currently a Professor. He has published more than 50 technical papers. He is primarily involved with the research and development of high-voltage vacuum circuit breakers.

Dr. Liu is a member of the Current Zero Club and a member of the CIGRE working group WGA3.27 "The impact of the application of vacuum switchgear at transmission voltages."

Dong Wang was born in Shaanxi Province, China, in 1983. He received the B.S. degree in electrical engineering from Xi'an Jiaotong University, Xi'an, China, in 2006, where he is currently working toward the M.S. degree in the State Key Laboratory of Electrical Insulation and Power Equipment, Department of Electrical Engineering.

He is involved with the research of vacuum arcs.

Mingzhe Rong (M'98) was born in Shanxi Province, China, in 1963. He received the B.S., M.S., and Ph.D. degrees in electrical engineering from Xi'an Jiaotong University, Xi'an, China, in 1984, 1987, and 1990, respectively.

He is currently a Professor with the State Key Laboratory of Electrical Insulation and Power Equipment, Department of Electrical Engineering, Xi'an Jiaotong University. Since 1984, he has been involved in the fields of arc physics, electrical contact theory, intelligent electrical apparatus, and condition monitoring technique for switchgear. He has published over 130 papers.

Dr. Rong is a member of the IEICE and the China Electrotechnical Society.